

Quenching of the Fluorescence from Chromium(III) Ions in Chromium-Doped Forsterite by an Aluminum Codopant

Jennifer L. Mass, James M. Burlitch,* David E. Budil, Jack H. Freed, Duane B. Barber,[†] Clifford R. Pollock,[†] Mikio Higuchi,[‡] and Rüdiger Dieckmann[‡]

Department of Chemistry, Baker Laboratory, Cornell University, Ithaca, New York 14853

Received January 6, 1995. Revised Manuscript Received February 17, 1995[⊗]

The H₂O₂-assisted sol-gel method was used to synthesize polycrystalline chromium and aluminum codoped forsterite powders with varying ratios of aluminum to chromium. These powders were used as feedstocks to grow single crystals by the floating zone method. The dopant composition of the resulting pleochroic crystals was determined by neutron activation analysis. Hyperfine splittings observed in the EPR study revealed that over half of the Cr³⁺ ions were present as chromium-aluminum pairs. The near-IR emission spectra of the crystals displayed the high ratios of Cr⁴⁺ to Cr³⁺ fluorescence intensities that have been previously reported for co-doped forsterite. Integration of the Cr⁴⁺ and Cr³⁺ EPR resonances, however, revealed that most of the chromium was in the 3+ oxidation state. The high ratio of Cr⁴⁺/Cr³⁺ emissions is attributed to quenching of the fluorescence from Cr³⁺.

Introduction

Chromium doped forsterite (Cr:Mg₂SiO₄) is a tunable, solid-state lasing material in the near infrared (1.1–1.3 μm) which has many promising applications in both the optical communications and biomedical fields.¹ Although the near IR lasing center in this material was initially the subject of much debate, recent findings indicate that the Cr⁴⁺ ion in a distorted tetrahedral site is the active center.^{1–4} The addition of codopants (intentionally or adventitiously) has been observed to have a significant impact upon the optical properties of the material.^{2,5} On one hand, Cr²⁺ and Fe³⁺ centers have been demonstrated to have parasitic absorbances in the near-IR region, which reduce the effectiveness of the laser. On the other hand, Al³⁺ centers have been reported to enhance the near-IR lasing properties of Cr:Mg₂SiO₄ by increasing the ratio of Cr⁴⁺ to Cr³⁺ emissions.⁶ The nature of this increase is poorly understood, and it has yet to be either quantified or optimized. The purpose of the present study is to investigate the role of the Al³⁺ codopant.

A H₂O₂-assisted, sol-gel method for the synthesis of homogeneous, transition-metal-doped, polycrystalline

forsterite was developed at Cornell University.^{7–9} Single-crystalline boules (~3 × 1 cm) were grown from the polycrystalline fired powders under oxidizing atmospheres using the floating zone method.¹⁰ These techniques were used to prepare crystals of forsterite doped with varying ratios of aluminum and chromium. This article describes the correlation of the optical properties of these crystals with their Al/Cr and Cr⁴⁺/Cr³⁺ ratios and proposes a new explanation for the apparent increase of the Cr⁴⁺ fluorescence intensity.

Experimental Section

General Comments. All sol-gel precursor synthesis was done under a scrubbed argon atmosphere on a double-manifold vacuum system.¹¹ Transfers of air- or moisture-sensitive materials were carried out in a N₂-filled glovebox (Vacuum Atmospheres Corp). Magnesium chips (99.95%), 2,4-pentanedione (99+%), and Al(OBu)₃ (97%) were obtained from Aldrich Chemicals, and were used as received. ACS grade methanol (Fisher Scientific) was freshly distilled from Mg(OMe)₂ prior to use. ACS grade 2-methoxyethanol (Fisher) was distilled over sodium prior to use. Chromium trioxide (CrO₃) and 30% hydrogen peroxide (H₂O₂) were obtained from Fisher Scientific and were used as received. Tetraethylorthosilicate (TEOS), 99+%, was used as received from Hüls America. Unless specified, all other chemicals were reagent grade.

VIS/near-IR spectra were recorded on a Varian Cary-5 spectrophotometer with a polarizing filter. The crystals used in this study were free of any observable defects, which might cause scattering. Polarizer and crystal alignments were carefully checked prior to each measurement. A Scintag PAD X diffractometer was used to obtain powder XRD patterns.

* To whom correspondence should be addressed.

[†] School of Electrical Engineering, Cornell University.

[‡] Department of Materials Science and Engineering, Cornell University.

[⊗] Abstract published in *Advance ACS Abstracts*, April 1, 1995.

(1) Petricevic, V.; Gayen, S. K.; Alfano, R. R.; Yamagishi, K.; Anzai, H.; Yamaguchi, Y. *Appl. Phys. Lett.* **1988**, *52*, 1040–1042.

(2) Petricevic, V.; Gayen, S. K.; Alfano, R. R. *Appl. Phys. Lett.* **1988**, *53*, 2590–2592.

(3) Yamaguchi, Y.; Yamagishi, K.; Nobe, Y. *J. Cryst. Growth*, **1993**, *128*, 996–1000.

(4) Casas-Gonzalez, J.; Jacobsen, S. M.; Hoffman, K. R.; Yen, W. M. *OSA Proc. Adv. Solid-State Lasers* **1991**, *10*, 64–68.

(5) Yamaguchi, Y.; Yamagishi, K.; Sugimoto, A.; Nobe, Y. *OSA Proc. Adv. Solid-State Lasers* **1991**, *10*, 52–56.

(6) Verdun, H. R.; Thomas, L. M.; Andrauskas, D. M.; Pinto, A. *OSA Proc. Tunable Solid State Lasers* **1989**, *5*, 85.

(7) Park, D. G.; Burlitch, J. M.; Geray, R. F.; Dieckmann, R.; Barber, D. B.; Pollock, C. R. *Chem. Mater.* **1993**, *5*, 518.

(8) Park, D. G. Ph.D. Thesis, Cornell University, 1994.

(9) Burlitch, J. M.; Becman, M. L.; Riley, B.; Kohlstedt, D. L. *Chem. Mater.* **1991**, *3*, 692–698.

(10) Higuchi, M.; Geray, R. F.; Dieckmann, R.; Park, D. G.; Burlitch, J. M.; Barber, D. B.; Pollock, C. R. *J. Cryst., Growth* **1995**, *148*, 140–147.

(11) Burlitch, J. M. How to Use Ace No-Air Glassware. *Bulletin* **3840**; Ace Glass Inc.: Vineland, NJ, 1984; pp 1–12.

Single-crystal boules were grown using a single ellipsoid image furnace (NEC SC-N35HS/50XS).¹⁰ Crystal orientation was performed using a real-time Laue backscattering diffractometer. Samples for neutron activation analysis (NAA) were irradiated in a TRIGA reactor operating at 300 kW. γ -ray spectrometry was performed using a coaxial Ortec HPGe detector with a planar face, which was 10 cm from the activated sample. Irradiations for NAA performed at the National Institute of Standards and Technology (NIST) used the NBS reactor operating at 15 MW. γ -ray spectrometry done at NIST utilized an Ortec LFC detector. X-band EPR spectra were obtained using a Bruker ER 200 D-SRC spectrometer.

Precursor Synthesis. TEOS (29.31 g, 0.1407 mol) was transferred via a cannula into a 100-mL Schlenk reaction vessel (SRV).¹¹ A dry 1-L three-necked round-bottom flask equipped with a water-cooled condenser, which was connected to a source of argon via a three-way stopcock, was charged with magnesium (6.841 g, 0.2815 mol) and 600 mL of MeOH. After all the Mg reacted and gas evolution ceased, the solution was filtered through a fritted filter tube (porosity D) into a 2-L round-bottom creased flask, which was equipped with a water-cooled condenser and a mechanical stirrer. The 1-L flask and the filter tube were rinsed with MeOH (3×50 mL). The TEOS in the 100-mL SRV was combined, with stirring, with the Mg(OMe)₂ solution via a cannula, and the SRV was also rinsed with MeOH (3×30 mL). The rinsings were then added to the reaction mixture.

CrO₃ pellets (0.0141 g, 1.41 mmol), weighed in the air, were transferred into a dry 100-mL SRV under a back-flow of argon. MeOH (100 mL) was added (via a syringe) to a mixture of the CrO₃ and 0.15 mL of distilled, deionized H₂O in a SRV. After the vigorous reaction ceased, the clear, dark reddish brown solution was combined with the alkoxide mixture. The 100-mL SRV was then rinsed with methanol (3×30 mL), and the rinsings were added via a cannula to the 2-L reaction flask.

The resulting light yellow mixture was hydrolyzed by the dropwise addition of a mixture of 14.99 g of 30% H₂O₂ (0.132 mol of H₂O₂ and 0.583 mol of H₂O) and 5.065 g of distilled, deionized water (0.2814 mol) in 400 mL of MeOH over the course of 72 h with vigorous stirring. Hydrolyzing agents were added via a cannula from a Schlenk tube that was pressurized by argon from a syringe in a syringe pump. The hazy greenish-yellow sol showed no tendency to precipitate.

In a glovebox, 0.104 g (0.4221 mmol) of Al(OBu^s)₃ was weighed into a 50-mL three-necked round-bottom flask. Under argon, freshly distilled 2-methoxyethanol (10 mL) was transferred via syringe into the flask. Over the course of 15 min 2,4-pentanedione (43 μ L, 0.4221 mmol) was added dropwise from a syringe to the reaction mixture, which was then stirred over an ice bath for 1 h. The resulting clear, pale yellow solution was then added via a cannula to the chromium-doped forsterite sol to give a greenish yellow codoped sol. The flask was rinsed with MeOH (3×10 mL), and the rinsings were added to the sol. The sol was stirred for 12 h before isolation of the xerogel.

The sols were converted to xerogels by heating (steam bath) during rotary evaporation under reduced pressure. Particles from the sol precursor for crystal 1 were precipitated by adding the sol dropwise to a 10:1 (v/v) stirred solution of distilled, deionized water and 30% ammonium hydroxide. The resulting pale yellowish green precipitate was filtered and washed repeatedly with distilled, deionized water. Xerogels obtained by both methods were reduced to a fine, bright yellow powder by grinding with an agate mortar and pestle.

Xerogels with different aluminum-to-chromium mole ratios and total dopant concentrations were prepared by the same general procedure except for the amount of chromium trioxide and aluminum precursor added (see Table 1). This study was conducted only on sols with Al/Si ratios less than 0.03 because sols prepared with an Al/Si ratio of greater than 0.03 were unstable and precipitated within 12 h.

Fired Powder Preparation and Single-Crystal Growth. The pale, yellowish green, codoped xerogel powders were precalcined at 200 °C in a vacuum oven under a humid air

Table 1. Initial Compositions of Cr,Al:Mg₂SiO₄ Precursor Sols for Single-Crystal Growth

crystal	Cr/Si ^a	Al/Si ^a	Al/Cr ^a
1	0.01	0.011	1.1
2	0.01	0.01	1.0
3	0.01	0.02	2.0
4	0.01	0.03	3.0
5	0.001	0.003	3.0

^a Molar ratio.

flow in order to facilitate the decomposition and evaporation of residual organics. Xerogels were calcined and fired in air for 6 h at 300 °C and 6 h at 1000 °C; the ramp rate was ~ 1.6 °C/min. The resulting fired powders were pale pink in the center of the fused silica boat and purple along the outer edges. A typical yield, based on TEOS, was 96%.

Bluish violet single-crystalline boules were grown at ~ 1890 °C from the fired powders using a floating zone technique.¹⁰ For crystal 1, a Ti-doped forsterite crystal, which had a Ti/Si mol ratio of 0.01, was used as a seed. For the remaining crystals, pieces of the boule from which crystal 1 was taken were oriented along the crystallographic *c*-axis (space group *Pnma*) and used as seeds. All crystals were grown in an atmosphere of 100% O₂ except for 5, which was grown in a mixture of 25% Ar and 75% O₂ (1 atm total pressure). The typical growth rate was 2 mm/h.

Single-crystal boules were oriented using real-time Laue X-ray backscattering and were cut perpendicularly to the three crystallographic axes using a diamond saw. The crystals displayed pleochroism identical to that of Cr:Mg₂SiO₄ with blue, violet, and green colors seen along the *a*, *b*, and *c*-axes, respectively. Crystals reserved for optical studies were polished down to 0.05 μ m using alumina polishing pads.

Neutron Activation Analysis. (1) *at Cornell University.* All samples were irradiated within $\frac{1}{8}$ dram polyethylene vials. Samples for aluminum analysis were transferred into unirradiated vials before counting. Fired powders were heat-sealed in the vial for chromium analysis and pressed into pellets for transfer when used for aluminum analysis. To measure Cr/Si ratios, γ -rays were counted from ⁵¹Cr and ³¹Si at 320.1 and 1266 keV, respectively. Optimum conditions for observing the former were an irradiation time of 30 min followed by a decay time of at least 1 h before counting. The ²⁸Al 1779 keV and the ²⁷Mg 1014 keV γ -rays were used to obtain Al/Mg ratios. Optimum conditions for observing aluminum were an irradiation time of 5 min, a decay time of 10 min, followed by a counting time of 20 min. Initially, aluminum-containing polymerization catalysts present in the polyethylene sample holders added to the ²⁸Al signal coming from the sample to give a false high reading. This problem was overcome by transferring the samples to new, unirradiated vials following activation. The ²⁸Al signal from the competing ²⁸Si(n,p)²⁸Al fast neutron reaction was taken into account by subtracting the ratio of ²⁸Al/²⁹Al produced by silicon-containing blanks from the ratio of ²⁸Al/²⁹Al produced by the Cr,Al:Mg₂SiO₄ samples (see Results and Discussion).

(2) *At NIST.* All samples were irradiated in heat-sealed polyethylene bags in Teflon sample holders. Each sample was transferred to an unirradiated bag and sample holder for counting. Irradiation, delay, and counting times were varied to suit the specific irradiation ports used.

Optical Spectroscopy. Fluorescence spectra were obtained using a pump laser at 1064 nm (YAG) or at 514.5 nm (argon ion) to excite the Cr,Al:Mg₂SiO₄ crystal. A scanning monochromator, with either a silicon or germanium detector, was used to record the resulting spectra.

Electron Paramagnetic Resonance. X-band EPR spectra of oriented single crystals were taken at 9.55 GHz with a nominal microwave power of 2.5 mW. Experimental parameters for rotational studies included a sweep time of 200 s, sweep width of 7000 G, and a time constant of 82 ms. Data collection parameters necessary to observe Cr-Al pairs were a sweep time of 500 s, a sweep width of 1000 G, and a time

constant of 160 ms. Data were acquired at 293 K on crystals with dimensions between 2 and 5 mm³. For quantitative measurement of the Cr⁴⁺/Cr³⁺ ratios, considerable care was exercised to ensure that peak areas were proportional to relative concentrations. The ratio of Cr⁴⁺/Cr³⁺ in each crystal was determined by EPR using the integration method developed by Budil et al.¹² In addition to correcting for the different transition probabilities, Boltzmann population distributions, and spin-lattice relaxation times of the two centers, it was also necessary to characterize the saturation behavior of each site with respect to crystal orientation. The higher field transitions ($-1/2$ to $+1/2$) for the octahedral M1 and M2 sites for Cr³⁺ were used for the integrations in accordance with the method of Budil et al. (see Figure 2).¹² Resonances from the chromium ions in all sites saturated at lower microwave powers when the spectrometer's magnetic field, **B**₀, was not aligned with a crystallographic axis. Consequently, integrations were performed on data collected in the crystallographic *ac* plane with **B**₀ parallel to the *a* axis for each crystal. Since peak intensities vary as a function of crystal orientation, integrated areas were corrected using a suitable factor from a previous rotational EPR study.¹²

Results and Discussion

Synthesis. The H₂O₂ assisted sol-gel synthesis of chromium-doped forsterite has been modified to allow for faster processing and for the inclusion of an aluminum codopant.⁷ Each step in the synthesis is designed to produce a stable, homogeneous mixture of the necessary metals, which will have the appropriate stoichiometry for the doped mineral product. The preparation of the magnesium and silicon alkoxide mixture is unchanged from previous procedures.⁷ The chromium dopant was prepared by the treatment of chromium(VI) oxide with distilled deionized water in methanol. Chromium trioxide is more convenient to use than chromium(II) acetate since; although it is hygroscopic, it is not subject to decomposition upon contact with oxygen in the atmosphere. The hydrolysis of the alkoxide and dopant mixture was accomplished in a one-step process by the slow addition of a dilute methanolic solution of 30% hydrogen peroxide (sufficient to hydrolyze 75% of the OR groups) and distilled deionized water (sufficient to hydrolyze 25% of the OR groups) to the reaction mixture. The sols that resulted from this abbreviated procedure were often cloudy but were stable with respect to precipitation.

AcacAl(OBu^s)₂ was chosen as a soluble source for an aluminum codopant and was added after the hydrolysis was completed in order to preserve the homogeneity of the sol.^{13,14} Unchelated Al(OBu^s)₃ is not a suitable aluminum precursor for a methanol-based sol since it will undergo alcohol exchange reactions leading to the formation of insoluble aluminum methoxides.¹⁴ The acacAl(OBu^s)₂ is added following the hydrolysis of the silicon and magnesium alkoxides since although chelating the metal will slow down its reactivity, it will eventually react to produce insoluble hydroxides.¹³ The synthesis and hydrolysis behavior of chelated aluminum alkoxides has been studied previously and applied to the synthesis of potassium fluorophlogopite.^{13,14}

UV-vis spectroscopy of an aliquot of the sol revealed strong absorbances at 290 and 370 nm. The 290 nm

absorbance is an agreement with a 287 nm absorbance reported for (acac)₃Al, and was assigned to the coordinated acetylacetonate moiety on this basis.¹⁵ The peak at 370 nm corresponds to the characteristic absorption for the chromate ion (Cr⁶⁺).^{16,17}

Following the addition of the aluminum dopant, the sol was stirred for at least 12 h to promote aging. For the Cr-doped sol, this process can be shortened by heating at reflux, but the aluminum-codoped sol is less stable and will precipitate upon heating. Evaporation of the solvent after aging resulted in the formation of a glassy, bright yellow xerogel. The ground xerogel powders were calcined and fired to 1000 °C in a box furnace to form polycrystalline codoped forsterite.

The variation in color of the codoped forsterite fired powder along the length of the fused silica boat (from purple to pale pink) is attributed to local inhomogeneities in the distribution of chromium oxidation states caused by poor circulation of the atmosphere within the furnace. The pyrolysis of residual organic groups in the xerogel during calcination may lead to the formation of carbon monoxide and, therefore, may create a slightly reducing atmosphere above the sample, which will affect the oxidation state of the final product.

Powder X-ray diffraction of the fired powders revealed polycrystalline forsterite free of any minor phases, i.e., (Al,Cr)₂O₃, and Mg(Al,Cr)₂O₄, for all concentrations of chromium and aluminum.

Single crystals were prepared by the floating zone method using a double melting technique to avoid bubble formation in the melt zone.¹⁰ The quality of the single-crystal boules that could be obtained from the forsterite powders was highly dependent upon dopant concentration. A boule totally free of imperfections (cracks, bubbles) was prepared from the fired powder that had the lowest initial dopant concentration (Cr/Si = 0.001, Al/Si = 0.003), whereas the feed rod from the fired powder with the highest initial dopant concentrations (Cr/Si = 0.01, Al/Si = 0.03) disintegrated during the initial melting.

Neutron Activation Analysis. Neutron activation analysis (NAA) of the fired powders revealed high levels of incorporation (greater than 90%) of both chromium and aluminum from the sol. As shown in Table 2, large losses of both dopants were observed, however, in the single crystals. The low chromium incorporation in the single crystal is the result of the formation of volatile chromium oxide such as CrO₃ in the oxidizing atmosphere.⁷ Aluminum, however, does not produce volatile oxides under these conditions, and therefore a different mechanism of dopant loss must be responsible. NAA of various sections of the boule from which crystal 2 was taken revealed that the concentration of aluminum increased dramatically along the rod moving away from the seed crystal despite the use of the double melting-technique to decrease zone-refining effects.¹⁰ The apparent loss of aluminum in crystals cut from portions of the boule adjacent to the seed crystal, therefore, is actually due to a displacement of aluminum from the growing boule by segregation into the melted phase.

(12) Budil, D. E.; Park, D. G.; Freed, J. H.; Burlitch, J. M.; Geray, R. F.; Dieckmann, R., *J. Chem. Phys.* **1994**, *101*, 3538–3548.

(13) Nass, R.; Schmidt, H. *J. Non-Cryst. Solids* **1990**, *121*, 329–333.

(14) Duldulao, F. D.; Burlitch, J. M. *Chem. Mater.* **1993**, *5*, 1037–1043.

(15) Singh, P. R.; Sahai, R. *J. Indian Chem. Soc.* **1969**, *46*(10), 945–955.

(16) Davies, W. G.; Prue, J. E. *Trans. Faraday Soc.* **1955**, *51*, 1045–1051.

(17) Johnson, L. W.; McGlynn, S. P. *Chem. Phys. Lett.* **1970**, *7*, 618–620.

Table 2. Neutron Activation Analyses of Single Crystals of Cr,Al:Mg₂SiO₄

crystal	Cr/Si ratio ^a (% incorp.) ^b	Al/Si ratio ^a (% incorp.) ^b	Al/Cr ratio ^a
1	$(8.5 \pm 1.3) \times 10^{-4}$ (8.5)	$(1.1 \pm 0.13) \times 10^{-3}$ (10)	1.3 ± 0.25
2	$(4.3 \pm 0.43) \times 10^{-4}$ (4.3)	$(3.5 \pm 0.35) \times 10^{-4}$ (3.5)	0.8 ± 0.11
3	$(8.9 \pm 1.2) \times 10^{-4}$ (8.9)	$(2.4 \pm 0.24) \times 10^{-3}$ (12)	2.7 ± 0.43
5	$(7.8 \pm 0.78) \times 10^{-5}$ (7.8)	$(6.9 \pm 1.4) \times 10^{-5}$ (2.3)	0.9 ± 0.2

^a Molar ratio ± error. ^b Incorporation values are relative to starting concentrations of dopants in the sol. ^c Measurement done using NIST reactor.

To determine the residual chromium present in the Cr,Al:Mg₂SiO₄ single crystals, the 320 keV ⁵¹Cr γ -ray intensity was compared to that from the 1266 keV ³¹Si γ -ray from the matrix. This method of analysis eliminated the need for precise measurements of the reactor flux and also the need for external chromium standards, which would be highly dependent upon reproducible irradiation and counting geometries. Aluminum concentrations were determined by an analogous method using the 1779 keV ²⁸Al and 1014 keV ²⁷Mg γ -rays.

Additional steps were necessary to obtain accurate analyses for aluminum due to a competing fast neutron reaction on the silicate matrix. This reaction, ²⁸Si(n,p)²⁸Al, added to the ²⁸Al signal coming from the desired ²⁷Al(n, γ)²⁸Al thermal neutron reaction. A new method of analysis, which relies solely on the inherent physical properties of the ²⁸Si and ²⁹Si nuclei, was developed to quantify this interference. Details of this method and results from analyses along the length of a boule will be presented elsewhere.¹⁸

EPR Studies. Despite the fact that the Cr⁴⁺ ion (ionic radius, 0.44 Å) is too large to fit in the site of Si⁴⁺ (ionic radius, 0.26 Å), the substitution of Cr⁴⁺ into the tetrahedral site of forsterite is well-established. Evidence for this substitution includes the work of Hoffman et al. in which the zero-field splittings of the tetrahedral Cr⁴⁺, determined by EPR, were compared with those deduced from the Zeeman effect on the narrow-line fluorescence peaks.¹⁹ In addition, the EPR parameters of Cr⁴⁺ in forsterite were shown by Garrett et al.²¹ to be very close to those of Cr⁴⁺ in akermanite, which has only tetrahedral substitution sites.²⁰ One explanation for the apparent ease of the Cr⁴⁺ for Si⁴⁺ substitution is that the Cr–O bonds are strongly covalent (i.e., the O²⁻ ions are not rigid but are polarizable), and so geometrical considerations based solely on ionic radii alone are not valid.⁶ EPR studies of Cr:Mg₂SiO₄ revealed that when Cr⁴⁺ substitutes for Si⁴⁺, the SiO₄ tetrahedron is compressed by a variable amount along the crystallographic *a* axis (space group, *Pnma*).¹²

X-band EPR spectroscopy of oriented, single-crystal-line Cr,Al:Mg₂SiO₄ revealed resonances from octahedral Cr³⁺ sites (M1 and M2), along with the resonance from the tetrahedral Cr⁴⁺ site, which has been previously observed in Cr:Mg₂SiO₄.^{7,23,26} The assignment of the Cr⁴⁺ resonance was confirmed by fitting the orientation dependence of the resonance to a calculated rotation pattern derived from the best-fit spin-Hamiltonian

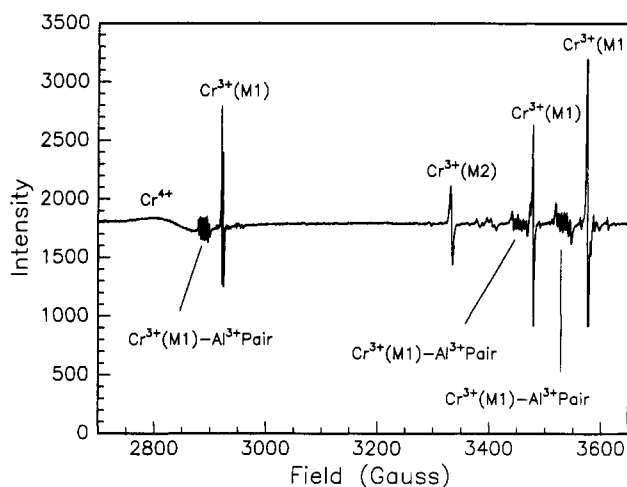


Figure 1. EPR spectrum (9.55 GHz) of oriented single crystal **2** with B_0 in the *bc* plane at an angle of 48° off the *b* axis (*Pnma*), showing resonances for Cr⁴⁺ and Cr³⁺. This orientation was selected to clearly display the resonances of the Cr³⁺–Al³⁺ pairs.

parameters. Additional confirmation of this assignment has been provided by extensive EPR experiments at 1.4–4.0 K.²² For crystals having high concentrations of dopants (all except **5**), an additional broadened resonance was observed adjacent to each Cr³⁺ peak. As shown in Figure 1, a characteristic, six-line, hyperfine splitting could be resolved for several of these resonances. The hyperfine splitting, caused by an interaction of the electron spin of Cr³⁺ with the nuclear spin of Al (*I* = 5/2), identifies these resonances as Cr³⁺–Al pairs.²³ Further characterization of these resonances by a full rotational study revealed that they have *D*, *E*, and Euler angles identical to those observed by Bershov et al.²³ The remaining broadened resonances (not shown), for which no hyperfine interactions could be resolved, are assigned as Cr³⁺–Cr³⁺ interactions.

To obtain the Cr⁴⁺/Cr³⁺ ratios, EPR spectra were integrated according to the procedure described in the Experimental Section. Integration of the resonances from crystal **5** was complicated by the presence of an additional resonance, possibly from Cr⁴⁺ not in a tetrahedral site. The angular dependence of this resonance at 34 GHz is currently under investigation.

The ratios of Cr⁴⁺ to Cr³⁺ ions observed by EPR in the codoped single crystals (see Table 3) show that

(18) Mass, J. L.; Burlitch, J. M.; McGuire, S.; Hossain, T. Z.; Demiralp, R. *Nucl. Instrum. Methods Phys. Res., Sect. A* **1994**, *353*, 606–609.

(19) Hoffman, K. R.; Casas-Gonzalez, J.; Jacobsen, S. M.; Yen, W. M. *Phys. Rev. B* **1991**, *44*, 12589.

(20) Rager, H. *Phys. Chem. Miner.* **1977**, *1*, 371–378.

(21) Garrett, M. H.; Chan, V. H.; Jessen, H. P.; Whitmore, M. H.; Sacra, A.; Singel, D. J.; Simkin, D. J. *OSA Proc. Adv. Solid State Lasers* **1991**, *10*, 76–80.

(22) Freed, J.; Tiram-Regev, A., to be submitted for publication.

(23) (a) Bershov, L. V.; Gaitte, J.-M.; Hafner, S. S.; Rager, H. *Phys. Chem. Miner.* **1983**, *9*, 95–101. (b) Kröger, F. A.; Vink, H. J. In *Solid State Physics—Advances in Research and Applications*. Seitz, F., Turnbull, D., Eds.; Academic Press: New York, 1957; Vol. 3, p 307–435.

(24) A detailed study of the Cr⁴⁺/Cr³⁺ ratio in Cr:Mg₂SiO₄ and its relationship to growth conditions and emission spectra is in progress. Results from this work and from point defect calculations on Cr,Al:Mg₂SiO₄ will be submitted for publication.

(25) Petricevic, V.; Gayen, S. K.; Alfano, R. R. *OSA Proc. Tunable Solid State Lasers* **1989**, *5*, 77–84.

(26) Jia, W.; Liu, H.; Jaffe, S.; Yen, W. M.; Denker, B. *Phys. Rev. B* **1991**, *43*, 5234–5242.

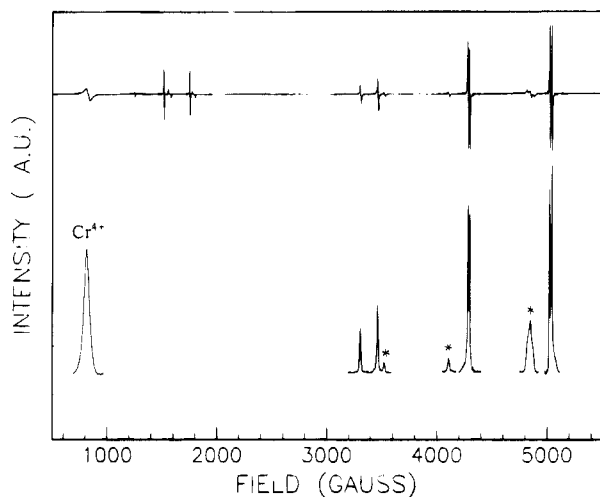


Figure 2. EPR Spectrum (9.55 GHz) of crystal 2 showing peaks (lower traces) from integration of the spectrum (upper scan). Areas under these peaks, after correction for rotation angle,¹² provided the basis for the calculation of the $\text{Cr}^{4+}/\text{Cr}^{3+}$ ratio. Peaks marked with an asterisk are from Cr^{3+} - Al^{3+} pairs.

Table 3. Cr^{3+} and Cr^{4+} Populations in $\text{Cr,Al:Mg}_2\text{SiO}_4$ Obtained by EPR

crystal	Cr^{3+} M1 site ^a	Cr^{3+} M2 site ^a	Cr^{4+} Td site ^a	$\text{Cr}^{4+}/\text{Cr}^{3+}$ ratio
1	69	17	14	0.16:1
2	45	11	44	0.79:1
3	54	17	29	0.41:1

^a Percentage of total chromium population.

substantial populations of Cr^{3+} ions are present in all crystals. This result is contrary to a report, based upon optical studies alone, that suggested aluminum codoping increased the concentration of Cr^{4+} .⁶ The presence of significant amounts of Cr^{3+} observed in the present work can be predicted using a charge compensation mechanism. Al^{3+} can be assumed to preferentially occupy a tetrahedral site due to its size and its known facile substitution for Si in many minerals. The resulting defect, $(\text{Al}^{3+}_{\text{Si}^{4+}})'$, has a net negative charge, which can be compensated by an adjacent defect, $(\text{Cr}^{3+}_{\text{Mg}^{2+}})^\bullet$ with a net positive charge.^{23a} The ionic Kröger-Vink notation is used to denote defect ionic species.^{23b} Qualitatively, the stabilization of the aluminum defect $(\text{Al}^{3+}_{\text{Si}^{4+}})'$ provides a driving force for an increase in the population of the $(\text{Cr}^{3+}_{\text{Mg}^{2+}})^\bullet$ centers over neutral $(\text{Cr}^{4+}_{\text{Si}^{4+}})^\times$ centers.²⁴

Optical Studies. Absorption and fluorescence spectra of the oriented and polished single crystals of $\text{Cr,Al:Mg}_2\text{SiO}_4$ were obtained to examine the effect of varying the concentration of the aluminum codopant. The polarized absorption spectra of crystal 1 (see Figure 3) displayed the prominent Cr^{4+} bands previously assigned by Petricevic et al.²⁵ for $\text{Cr:Mg}_2\text{SiO}_4$ and by Verdun et al.⁶ for $\text{Cr,Al:Mg}_2\text{SiO}_4$. For example, the latter authors reported 1083 and 741 nm for the most intense components of the ${}^3\text{A}_2 \rightarrow {}^3\text{T}_2$ and ${}^3\text{A}_2 \rightarrow {}^3\text{T}_1$ transitions, respectively. These values are similar to those shown in Table 3 (1073 and 740 nm, respectively). Using site-selective excitation spectroscopy, Jia et al. reported 738 nm for the most intense component of the ${}^3\text{A}_2 \rightarrow {}^3\text{T}_1$ transition.²⁶ These authors reported the ${}^4\text{A}_2 \rightarrow {}^4\text{T}_1$ transition of Cr^{3+} in the M2 site to be at 474 nm.

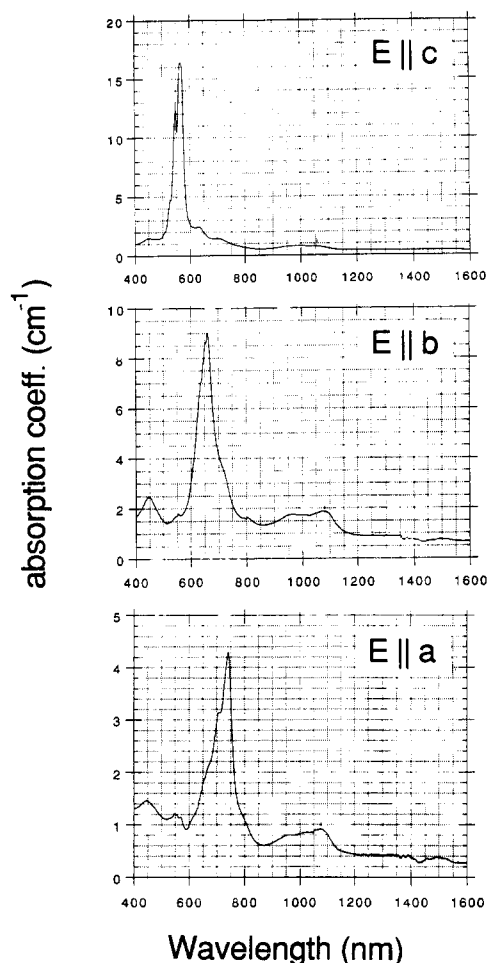


Figure 3. Polarized VIS-near-IR absorption spectra of $\text{Cr,Al:Mg}_2\text{SiO}_4$ crystal 1, the incident beam passes through the b axis ($Pnma$) and $E||a$.

Table 4. Absorption Maxima and Assignments for $\text{Cr,Al:Mg}_2\text{SiO}_4$

transition	peak (nm)		
	$(E a)$	$(E b)$	$(E c)$
Crystal 1			
${}^3\text{A}_2 \rightarrow {}^3\text{T}_2$	1073	1077	1055
${}^3\text{A}_2 \rightarrow {}^3\text{T}_1$	740	663	565
${}^4\text{A}_2 \rightarrow {}^4\text{T}_1$	448	449	450
Crystal 2			
${}^3\text{A}_2 \rightarrow {}^3\text{T}_2$	1078	1063	1065
${}^3\text{A}_2 \rightarrow {}^3\text{T}_1$	740	660	560
${}^4\text{A}_2 \rightarrow {}^4\text{T}_1$	440	425	
Crystal 3			
${}^3\text{A}_2 \rightarrow {}^3\text{T}_2$	1070	1075	1080
${}^3\text{A}_2 \rightarrow {}^3\text{T}_1$	740	660	565
${}^4\text{A}_2 \rightarrow {}^4\text{T}_1$	440	425	450

Thus, the band at ~ 450 nm (Figure 3 and Table 4) is assigned to the ${}^4\text{A}_2 \rightarrow {}^4\text{T}_1$ transition of Cr^{3+} .

Ratios of intensities of Cr^{4+} absorption bands to those of Cr^{3+} were qualitatively similar to those reported by Verdun et al.⁶ The decreased intensity of Cr^{3+} bands in Cr -doped forsterite has been observed previously: Lehmann pointed out that Cr^{3+} in forsterite is in a site of a larger host ion (Mg^{2+}), and the average intensities for the ligand field transitions are smaller than usual.²⁷ Another potential complication for the interpretation of absorption intensities is the number of species present.

(27) Lehmann, G. *Chem. Phys. Lett.* **1979**, *65*, 184-186.

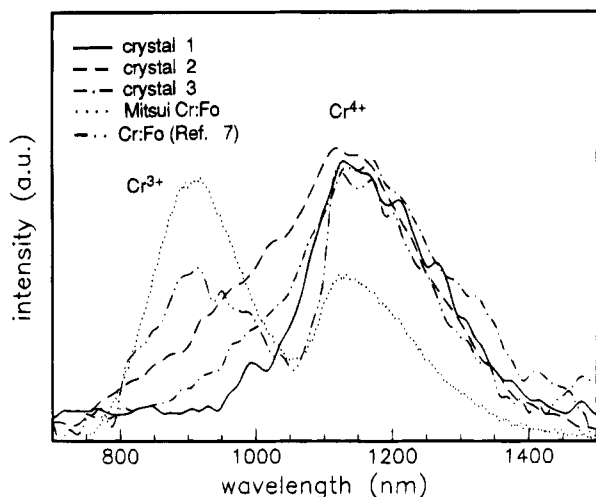


Figure 4. Argon laser pumped emission spectra for Cr:Mg₂SiO₄ and Cr,Al:Mg₂SiO₄ samples grown in O₂ (1 atm total pressure); the beam from the pump laser is along the *a* axis, and *E* is parallel to the *c* axis. The commercial crystal was obtained from the Mitsui Mining and Smelting Co.

For Cr³⁺, there are at least five possibilities: unpaired Cr³⁺ on M1 and M2 octahedral sites, Cr–Al pairs on these same sites, and Cr³⁺–Cr³⁺ interactions, as observed by EPR (see above). The Cr–Al pairs might have different intensities and energies from unpaired Cr³⁺ ions depending on the difference of charge overlap between O²⁻ and Cr³⁺ caused by the neighboring defect, viz., (Al³⁺Si⁴⁺)'.²⁷ Crystal 3 displayed a higher intensity ratio of Cr⁴⁺ to Cr³⁺ absorption bands than either chromium-doped forsterite or the other codoped samples; the band at 450 nm was barely visible. This sample also had the highest ratio of Al/Cr by NAA (see Table 2), and for the reasons noted above, viz., the formation of various defects, this correlation supports the notion that the aluminum codopant alters the Cr³⁺ absorption mechanism.

The fluorescence behavior of Cr:Mg₂SiO₄ has been examined in detail, and the emissions observed for the Cr,Al:Mg₂SiO₄ crystals in this study are interpreted by comparison with the reported data. Fluorescence spectra obtained at ambient temperature by excitation at 514.5 nm revealed two broad bands, centered at 900 and 1150 nm (see Figure 4). Together, these bands extend from 700 to 1500 nm. The band centered at 1150 nm has been attributed to the ³T₂ → ³A₂ transition of the Cr⁴⁺ ion in an Si⁴⁺ site and the band centered at 900 nm has been attributed to the ⁴T₂ → ⁴A₂ transition of the Cr³⁺ ions in the M1 and M2 octahedral sites.^{25,28}

All emission spectra of Cr,Al:Mg₂SiO₄ samples displayed Cr⁴⁺ emissions that ranged in intensity from equivalent to the Cr³⁺ emission to over 20 times more intense. In some spectra, the emission from Cr³⁺ was negligible or missing altogether. The spectrum from crystal 2 (Figure 4) displayed the highest ratio of Cr⁴⁺ to Cr³⁺ emissions, which is consistent with the Cr⁴⁺/Cr³⁺ ratio determined by EPR (see Table 3). Judging by peak intensity alone (Figure 4), Cr:Mg₂SiO₄, grown

under similar conditions, appears to have relatively more Cr³⁺ than Cr,Al:Mg₂SiO₄.²⁴

In a previous study of Cr,Al:Mg₂SiO₄ fibers grown by the laser-heated pedestal growth method, high ratios of Cr⁴⁺/Cr³⁺ emissions were also observed.⁶ The authors postulated that aluminum somehow "facilitated the incorporation of Cr(IV) into the forsterite crystal".⁶ The low ratios of Cr⁴⁺/Cr³⁺ observed by EPR in this study, however, indicate that aluminum may actually decrease the amount of Cr⁴⁺ present in the codoped crystal. Thus, the high ratio of Cr⁴⁺/Cr³⁺ fluorescence intensities observed is a result of a reduction in the intensity of the Cr³⁺ emission and not of an increase in the Cr⁴⁺ population. Since a significant portion of the Cr³⁺ centers in the present crystals occurred in Cr–Al pairs (see Figure 1), one possible conclusion is that Cr³⁺–Al³⁺ interactions are involved in the quenching of the Cr³⁺ emission band. The defect, (Al³⁺Si⁴⁺)' has an opposite effective charge from that of the adjacent (Cr³⁺Mg²⁺)' defect. Thus, the Al³⁺ ion in such a Cr–Al pair very likely has a strong electrostatic interaction with the (Cr³⁺Mg²⁺)' defect. Distortion of the Cr³⁺ center in (Cr³⁺Mg²⁺)' due to the presence of the defect, (Al³⁺Si⁴⁺)', could increase the possibility for an excited state of Cr³⁺ to decay by a nonradiative relaxation mechanism such as phonon-aided decay. A reviewer has suggested a mechanism in which a Cr³⁺–Al³⁺ pair associates with a Cr⁴⁺ ion resulting in a facilitated transfer of excitation from Cr³⁺ to Cr⁴⁺. Such a mechanism is possible, but there is no obvious (Coulombic) driving force for such an association to occur.

There does not appear to be a simple correlation between the NAA determined Al/Cr ratio and the Cr⁴⁺/Cr³⁺ ratio or the qualitative ratio of Cr⁴⁺ to Cr³⁺ from the emission spectra.³⁰ The crystal with the highest Al/Cr ratio, 3, displayed an intermediate Cr⁴⁺/Cr³⁺ ratio by EPR analysis and also an intermediate ratio of Cr⁴⁺/Cr³⁺ emissions. This lack of correlation suggests that there is an optimum Al/Cr ratio that produces the observed Cr³⁺ emission quenching. If Cr–Al interactions in Cr³⁺–Al pairs are responsible for the fluorescence quenching, then a Al/Cr ratio approaching unity should be sufficient to maximize this effect. However, crystals 1 and 2, which have Al/Cr ratios of approximately one, show significantly different ratios of Cr³⁺ and Cr⁴⁺ and emission spectra (Figure 2). Therefore, there must be an additional mechanism responsible for Cr³⁺ quenching.

A second mechanism that could produce fluorescence quenching and therefore perturb the Cr⁴⁺/Cr³⁺ emission ratio may be related to the total concentration of dopants in each sample.³¹ Quenching of the fluorescence from Cr³⁺ has been observed in Cr:Mg₂SiO₄ at concentrations of chromium similar to those in the codoped samples. Therefore, effects of the total dopant concentration, not just the Al/Cr ratio, must be considered when comparing Cr⁴⁺/Cr³⁺ emission ratios. However, Table 2 and Figure 4 reveal that crystal 2 has the smallest overall dopant concentration and yet the largest Cr³⁺ quenching effect. Therefore, a concentration

(28) Moncorgé, R.; Cormier, G.; Simkin, D. J.; Capobianco, J. A. *IEEE J. Quantum Electron.* **1991**, *27*, 114–120.

(29) Moncorgé, R.; Manaa, X. X. *OSA Proc. Adv. Solid State Lasers* **1989**, 243–251.

(30) To ensure that the Cr/Al ratio, determined by NAA, was representative of that in the EPR sample, the sample for NAA was cut from an adjacent section of the boule. The 28 day half-life of ⁵¹Cr made it difficult to use one sample for both analyses.

(31) Dexter, D. L.; Schulman, J. H. *J. Chem. Phys.* **1954**, *22*, 1063–1070.

quenching mechanism appears not to dominate the properties of the emission spectra but still may be a factor, in conjunction with effects based upon chromium and aluminum interactions.

Summary and Conclusions

The procedure for the sol-gel synthesis of chromium-doped forsterite was modified to produce chromium and aluminum codoped forsterite. EPR studies of single crystals revealed the presence of $\text{Cr}^{3+}-\text{Al}^{3+}$ pairs. The codoped samples, grown in oxygen, were shown by EPR to contain ratios of Cr^{4+} to Cr^{3+} that were less than unity. The codoped crystals displayed high ratios of $\text{Cr}^{4+}/\text{Cr}^{3+}$ emissions, however, despite relatively low concentrations of the Cr^{4+} ion. This discrepancy is

attributed to a quenching of the Cr^{3+} emission, most likely caused by both $\text{Cr}^{3+}-\text{Al}$ interactions and concentration quenching by other chromium ions.

Acknowledgment. The authors thank the Cornell University Materials Science Center (NSF: DMR 9121654) and the AT&T Foundation for financial support and appreciate assistance from the following: Prof. Stephen S. McGuire and Dr. Tim Z. Hossain provided advice on NAA methods at Cornell and Dr. Rabia Demiralp helped with the NAA experiments performed at NIST. Prof. H. Rager gave helpful suggestions on possible roles of Cr-Al pairs.

CM9500115